PIER C

(Received 1 July 2025, Accepted 9 October 2025, Scheduled 18 October 2025)

# Fast Voltage Stabilization Control of Dual Three Phase Permanent Magnet DC Power Generation System for Flywheel Energy Storage

Xinjian Jiang[1], Zhijian Ling[2,*], Fuwang Li[1], Zhenghui Zhao[2], and Zhiru Li[1]

[1] *Shanxi Energy Internet Research Institute, Taiyuan 030000, China*
[2] *School of Electrical and Information Engineering, Jiangsu University, Zhenjiang 212013, China*

**ABSTRACT:** This paper proposes a fast voltage regulation control method based on direct power calculation. To suppress the issues of long bus voltage recovery time and large voltage fluctuation in dual three-phase permanent magnet generator, firstly, in the voltage outer loop, the fast adjusting component of the inner loop power reference is derived through a direct power calculation method. This approach enhances the dynamic response of the bus voltage. Secondly, to mitigate control errors induced by system losses, a capacitor power compensation method is introduced to generate an error compensation component for the power reference, thereby improving the voltage control accuracy. Finally, the feasibility and effectiveness of the proposed control strategy are validated through both software simulations and experimental tests. In comparison with conventional methods, the proposed strategy provides stronger disturbance rejection and a faster dynamic response, enabling high-performance DC bus voltage control for dual three-phase permanent magnet generator systems.

## 1. INTRODUCTION

As a representative of physical energy storage technologies, flywheel energy storage has demonstrated unique advantages in recent years, particularly in high-performance and high-frequency application scenarios [1–3]. Owing to its fast response, high short-term power output, high reliability, instantaneous energy absorption, and rapid energy release, flywheel energy storage performs well in applications such as grid frequency regulation, hybrid energy storage systems, data center UPS, and regenerative braking in rail transit systems [4–7]. DTP-PMSG rectification system, through multiphase winding decoupling and high-speed electromagnetic control, addresses issues such as harmonic suppression and precise torque regulation during the charging and discharging processes of flywheel energy storage [8–11]. However, when the DC-side load of the rectification system undergoes sudden changes, significant fluctuations in the bus voltage may occur, which in severe cases can even lead to system collapse [12, 13]. Such events seriously affect the safety of both the rectifier and flywheel energy storage device, highlighting the need for generator fast voltage regulation control methods targeting sudden load power changes, so as to ensure the reliability and safety of the generation-rectification system.

When a DTP-PMSG rectification system adopts the dual closed loop control strategy for voltage and power, the bus voltage acts as the controlled variable of the outer loop, while the power serves as the controlled variable of the inner loop [14]. In conventional control methods, a proportional-integral (PI) controller is used in the system's outer loop, resulting in limited dynamic performance. Under harsh DC-side load conditions (such as large-capacity sudden load changes), the system output bus voltage is prone to large fluctuations and prolonged voltage recovery times, thus weakening the control performance. Therefore, to enhance the dynamic performance of the bus voltage and improve the system's ability to withstand load disturbances during sudden load changes, it is necessary to accelerate the dynamic response of the system [15, 16]. Currently, in response to these issues, researchers have proposed advanced control methods, such as load power feedforward [17], sliding mode control [18–20], disturbance observer-based compensation control [21, 22], nonlinear control [23], backstepping control [24], and predictive control [25–27].

In [17], the product of the bus voltage and load current is used in the voltage outer loop to obtain the load power, which is then superimposed on the output of the bus PI controller as the reference value for active power. This approach improves the dynamic performance of the bus voltage, but the feedforward part does not account for the variation in DC-side capacitor power during load addition or removal, presenting certain limitations. Ref. [18] applies sliding mode control based on a load current observer to generate the inner loop active power reference, which improves system dynamic performance; however, the approach law in the sliding mode control requires further improvement to increase the convergence speed to the sliding manifold, and the enhancement in bus voltage response speed is limited. Ref. [19] designs a sliding mode controller based on an adaptive super-twisting approach, resolving the contradiction between dynamic characteristics and chattering in sliding mode control and improving system dynamic and static performance,

* Corresponding author: Zhijian Ling (lzj1991@ujs.edu.cn).

albeit with a complex design process for dynamic adaptive gain. Refs. [21, 22] use disturbance observers to estimate system disturbances and feed these estimates forward to the outer voltage controller, thereby mitigating the adverse effects of load disturbances and improving DC-side voltage tracking performance. However, the large number of parameters to be tuned in the observer makes the actual tuning process cumbersome. Ref. [24] introduces two Lyapunov functions in the voltage outer loop to design a backstepping controller for the bus voltage, enhancing the system's ability to resist load disturbances. However, the sign function in the backstepping control is not optimized, leading to significant chattering.

This paper improves the outer loop control strategy for a DTP-PMSG rectification system and proposes a fast voltage regulation control strategy based on direct power calculation. On one hand, the voltage outer loop directly calculates the reference value for the power inner loop according to the generator power balance equation, thereby improving the dynamic response speed of the voltage outer loop. On the other hand, capacitor power compensation is employed to eliminate the control error caused by direct power calculation, thus achieving zero steady-state error control of the bus voltage. Finally, the feasibility of the proposed control method is verified through simulation and experimental studies on the DTP-PMSG rectification system.

## 2. TOPOLOGY AND DTP-PMSG SYSTEM MODEL

A block diagram of the DTP-PMSG rectification system, which is centered on the DTP-PMSG and PWM rectifier, is shown in Fig. 1. This system primarily consists of a DTP-PMSG, a PWM rectifier, and a downstream load. The mechanical energy from the prime mover is ultimately converted into direct current through the generator and rectifier, which can then be supplied to downstream electrical devices.

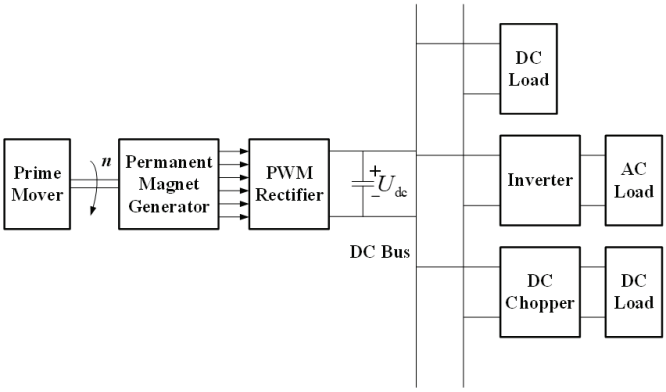


**FIGURE 1**. Block diagram of permanent magnet generator rectification system.

In the block diagram of the DTP-PMSG rectification system, the permanent magnet generator and rectifier are key components. The main circuit structure is illustrated in Fig. 2. The generator employs a DTP-PMSG with isolated neutral points, while the rectifier utilizes a two-level, six-phase voltage-source PWM rectifier. Here, $i_C$, $i_L$, and $i_{dc}$ denote the capacitor current, load current, and bus current, respectively. $R_L$ and $C$ represent the load resistance and DC-side capacitance.

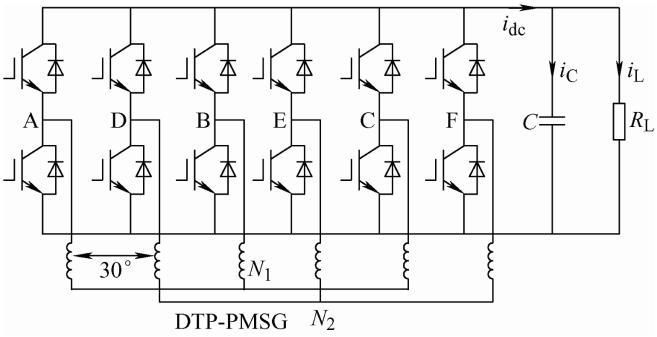


**FIGURE 2**. Main circuit diagram of DTP-PMSG rectification system.

The voltage equations of the dual three-phase permanent magnet generator in the natural coordinate system are transformed using a decoupling matrix:

$$\mathbf{T}_{\mathrm{CTM}} = \frac{1}{3}\begin{bmatrix} 1 & -\frac{1}{2} & -\frac{1}{2} & \frac{\sqrt{3}}{2} & -\frac{\sqrt{3}}{2} & 0 \\ 0 & \frac{\sqrt{3}}{2} & -\frac{\sqrt{3}}{2} & \frac{1}{2} & \frac{1}{2} & -1 \\ 1 & -\frac{1}{2} & -\frac{1}{2} & -\frac{\sqrt{3}}{2} & \frac{\sqrt{3}}{2} & 0 \\ 0 & -\frac{\sqrt{3}}{2} & \frac{\sqrt{3}}{2} & \frac{1}{2} & \frac{1}{2} & -1 \\ 1 & 1 & 1 & 0 & 0 & 0 \\ 0 & 0 & 0 & 1 & 1 & 1 \end{bmatrix} \tag{1}$$

where $\boldsymbol{T}_{\mathrm{CTM}}$ represents the Clarke transformation matrix. As a result, the voltage equations of the generator in the stationary coordinate system are obtained:

$$\begin{cases} u_\alpha = e_\alpha - R_s i_\alpha - L_\alpha \dfrac{di_\alpha}{dt} \\ u_\beta = e_\beta - R_s i_\beta - L_\beta \dfrac{di_\beta}{dt} \\ u_x = -R_s i_x - L_x \dfrac{di_x}{dt} \\ u_y = -R_s i_y - L_y \dfrac{di_y}{dt} \end{cases} \tag{2}$$

In these equations, $u_\alpha$ and $u_\beta$ denote $\alpha$-$\beta$ axis components of the stator voltage, while $u_x$ and $u_y$ represent $x$-$y$ axis components of the stator voltage. Similarly, $i_\alpha$ and $i_\beta$ represent $\alpha$-$\beta$ axis components of the phase current, while $i_x$ and $i_y$ correspond to $x$-$y$ axis components. $L_\alpha$ and $L_\beta$ are $\alpha$-$\beta$ axis components of the stator inductance, while $L_x$ and $L_y$ are $x$-$y$ axis components of the stator inductance. $e_\alpha$ and $e_\beta$ are $\alpha$-$\beta$ axis components of the back electromotive force (EMF), and $R_s$ is the stator resistance.

The expression for the instantaneous power of the generator in the stationary coordinate system is as follows:

$$\begin{cases} P = 3(e_\alpha i_\alpha + e_\beta i_\beta) \\ Q = 3(e_\beta i_\alpha - e_\alpha i_\beta) \end{cases} \tag{3}$$

where $P$ and $Q$ are the active and reactive powers of the generator, respectively. The expressions for $e_\alpha$ and $e_\beta$ are given by:

$$\begin{cases} e_\alpha = E\cos\theta \\ e_\beta = E\sin\theta \end{cases} \tag{4}$$

where $E$ is the amplitude of the generator's back EMF, and $\theta$ is the angle between the back EMF and phase A. The expressions for $E$ and $\theta$ are:

$$\begin{cases} E = \omega_e \psi_f \\ \theta = \theta_e + \dfrac{\pi}{2} \end{cases} \tag{5}$$

where $\omega_e$ is the electrical angular velocity of the generator, $\psi_f$ the flux linkage of the permanent magnet, and $\theta_e$ the electrical angle of the generator.

As indicated by Eq. (3), when the inner loop of the permanent magnet generator rectification system uses power as the controlled variable, the active and reactive power produced by the generator can be controlled independently. By employing a control strategy with $Q^* = 0$, the power factor of the generator can be improved, thereby increasing the efficiency of the machine and reducing losses in the power generation system.

## 3. VOLTAGE STABILIZATION CONTROL STRATEGY

### 3.1. Principle of Voltage Stabilization Control Strategy

In DTP-PMSG rectification system, a dual closed loop control strategy based on voltage and power is adopted. The outer loop of the power generation system uses bus voltage feedback as controlled variable, while the inner loop uses instantaneous power feedback as controlled variable. The voltage regulation process of the DTP-PMSG operates as follows: first, the voltage outer loop controller generates the active power reference for the inner loop based on the difference between the reference and actual bus voltages. To improve the generator's power factor and reduce harmonic current, both the reactive power reference and harmonic current reference are set to zero. Next, the power inner loop controller generates $\alpha$-$\beta$ axis voltage references $u_\alpha^*$ and $u_\beta^*$ according to the given power and calculated instantaneous power. These are then combined with harmonic voltage references $u_x^*$ and $u_y^*$. Using space vector pulse width modulation, twelve switching signals required for the six-phase PWM rectifier are obtained, ultimately achieving controllable bus voltage of the generator.

In conventional dual closed loop voltage-power control method, outer voltage loop employs a PI controller. Fig. 3 illustrates the conventional method used in the voltage outer loop. The conventional voltage outer loop controller takes the error between the bus voltage reference and feedback as the input to the bus voltage PI controller and multiplies the output by the actual bus voltage to obtain the power reference for the system's inner loop. Due to the lag inherent in PI control and the failure to account for nonlinear characteristics of the power equations in the generation system, this method results in large voltage fluctuations, prolonged recovery times, and poor disturbance rejection capability when the load changes suddenly.

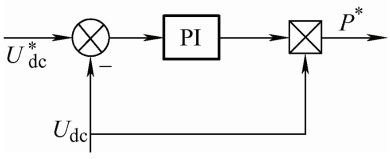


**FIGURE 3**. Schematic diagram of the conventional voltage outer loop method.

To address these issues, this paper proposes a rapid voltage regulation control method for permanent magnet generators based on direct power calculation. In the voltage outer loop, a control strategy based on direct power calculation and capacitor power compensation is adopted. The fast adjustment component of the active power reference for the inner loop is directly calculated to accelerate the recovery of the bus voltage and reduce its fluctuation amplitude in the DTP-PMSG rectification system. Subsequent simulations and experiments compare and analyze the performance of the proposed method with that of the conventional approach.

### 3.2. Voltage Outer Loop Control Strategy

The objective of the outer voltage control loop in a permanent magnet power generation system is to ensure that the actual bus voltage follows the reference bus voltage and remains relatively stable. The proposed outer loop control strategy consists of two main components: direct power calculation and capacitor power compensation. Direct power calculation accelerates the dynamic response of the outer loop bus voltage, while capacitor power compensation enhances the control accuracy of the bus voltage.

According to the Kirchhoff's Current Law, the DC-side current balance equation of the generation-rectification system is as follows:

$$i_{dc} = i_L + i_C \tag{6}$$

The current through the capacitor and the capacitor voltage have a differential relationship, which can be expressed as:

$$i_C = C\frac{dU_{dc}}{dt} \tag{7}$$

where $U_{dc}$ is the DC-side bus voltage of the generation system.

The expression for the DC-side power of the generation system is:

$$P_{dc} = U_{dc} i_{dc} \tag{8}$$

where $P_{dc}$ is the DC-side power of the generation system. Combining Eqs. (6) to (8), we obtain:

$$P_{dc} = U_{dc} i_{dc} = U_{dc} i_L + \frac{1}{2} C \frac{dU_{dc}^2}{dt} \tag{9}$$

If the losses in the rectifier and other losses in the generation system are neglected, the output power on the generator side is approximately equal to the DC-side power of the system:

$$P_1 = P_{dc} \tag{10}$$

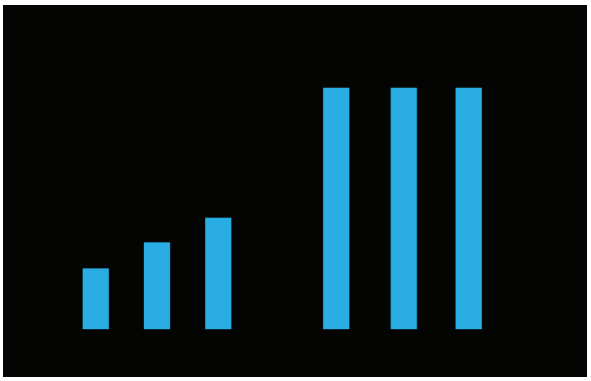

**FIGURE 4**. Schematic diagram of the capacitor charging process.

where $P_1$ is the generator-side output power.

Combining Eqs. (9) and (10), the inner loop power calculation formula based on direct power calculation can be derived as:

$$P_1 = U_{dc} i_L + \frac{1}{2} C \frac{dU_{dc}^2}{dt} \tag{11}$$

In practical generation systems, digital control units such as digital signal processor (DSP) are commonly used. Discretizing Eq. (11), the reference value for the inner loop power based on direct power calculation is:

$$P_1^* = U_{dc}^* i_L + \frac{1}{T_C} \left( \frac{1}{2} C U_{dc}^{*2} - \frac{1}{2} C U_{dc}^2 \right) \tag{12}$$

where $P_1^*$ is the reference value for the inner loop power obtained by direct power calculation, $U_{dc}^*$ the reference bus voltage on the DC-side, and $T_C$ the estimated time for the capacitor to reach the reference energy level. The design principle and selection criteria for the parameter $T_C$ are explained below.

When the system reaches a steady state, the rectifier outputs a constant voltage, so the DC-side can be equivalently modeled as a first-order circuit consisting of a voltage source, a capacitor, and a resistor. According to the circuit theory, the time constant of this circuit is:

$$\tau = RC \tag{13}$$

The design of the estimated time $T_C$ for the capacitor to reach the reference energy level is based on this time constant. Select $T_C = NT_s$ as the capacitor energy storage regulation time. $T_s$ is the control period, and $N$ is an integer, used to adjust the number of control periods. Taking the capacitor charging process as an example, the process is illustrated in Fig. 4.

At the $k$-th moment, the actual capacitor energy storage $E_C$ is less than the reference value $E_C^*$. It is assumed that after voltage regulation for a duration of $T_C$, the actual capacitor energy storage will reach the reference value. According to Eq. (12), the required charging power for the capacitor at this moment determines the active power reference value associated with capacitor charging. At the $(k+1)$-th moment, the new energy storage value is used to calculate the updated required charging power, and the active power reference value for capacitor

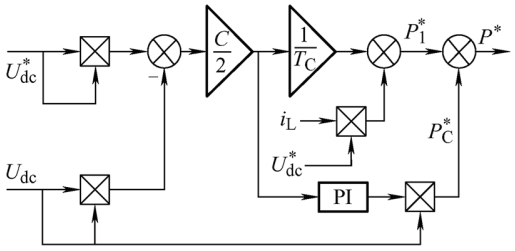


**FIGURE 5**. Schematic diagram of proposed voltage outer loop method.

charging is adjusted accordingly. This process is repeated iteratively. As the actual capacitor energy storage gradually increases, the charging power decreases step by step, eventually reaching the reference value. When the capacitor is discharging, a similar analysis applies and will not be repeated here.

The above analysis indicates that if $T_C$ is set too large, the actual energy storage will reach the reference value more slowly, which is detrimental to the rapid regulation of the DC bus voltage. Conversely, if $T_C$ is set too small, it facilitates faster adjustment of the capacitor energy storage but may also cause voltage oscillations, thus compromising the system's stability. Therefore, the parameter $T_C$ should be selected to balance the dynamic performance of the bus voltage and the relative stability of the system.

Therefore, as shown by Eq. (12), in contrast to using only a conventional PI controller in the voltage outer loop, the reference power is calculated directly, enabling a faster dynamic response of the voltage outer loop to sudden load changes.

To compensate for the control errors caused by system losses, a compensation component for the reference power is proposed based on direct power calculation and capacitor power compensation. This approach achieves zero steady-state error control of the bus voltage. The compensation component of the power reference is given as follows:

$$\begin{cases} E_C = \dfrac{1}{2} C U_{dc}^2 \\ E_C^* = \dfrac{1}{2} C U_{dc}^{*2} \\ P_C^* = U_{dc} \left[ k_p \left( E_C^* - E_C \right) + k_i \displaystyle\int \left( E_C^* - E_C \right) dt \right] \end{cases} \tag{14}$$

where $E_C^*$ is the reference value of capacitor energy storage, $E_C$ the feedback value, $P_C^*$ the compensation component of the power reference, $k_p$ the proportional constant, and $k_i$ the integral constant of the capacitor power PI controller.

The reference value for the inner power loop consists of two parts: the first is the fast adjustment component $P_1^*$ obtained by direct power calculation, and the second is the error compensation component $P_C^*$ produced by the output of the capacitor power PI controller. In summary, the reference value for the power inner loop can be expressed as follows:

$$P^* = P_1^* + P_C^* \tag{15}$$

A schematic diagram of the voltage outer loop based on direct power calculation proposed in this paper is shown in Fig. 5.

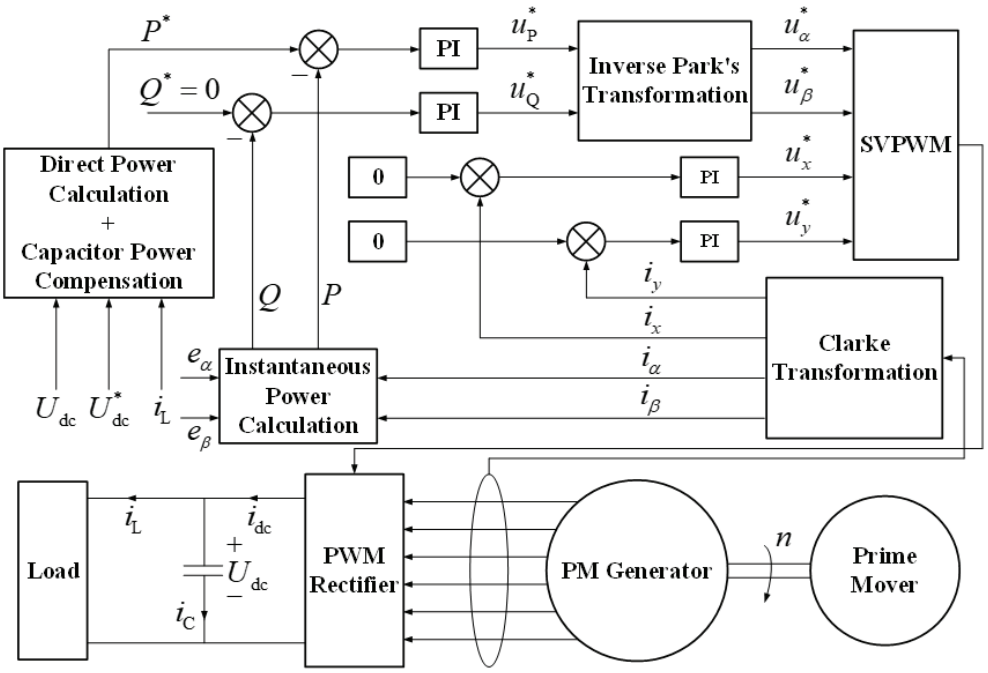


**FIGURE 6**. Control block diagram of DTP-PMSG rectification system.

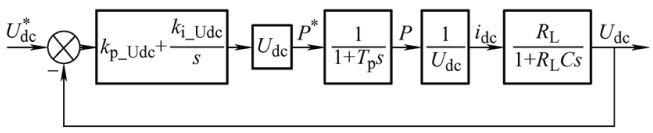

**FIGURE 7**. Bus voltage outer loop control block diagram using conventional PI control.

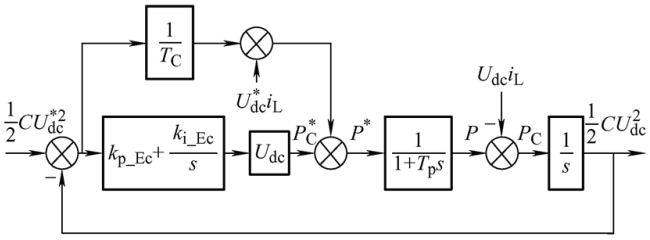

**FIGURE 8**. Bus voltage outer loop control block diagram of the proposed control method.

In the proposed method, $P_1^*$ is the fast adjustment component of the inner active power reference. Its function is to improve the dynamic performance of the voltage outer loop by direct power calculation, thereby enhancing the disturbance rejection capability of the DC-side voltage of the permanent magnet generator system under sudden load conditions. $P_C^*$ serves as the error compensation component of the inner active power reference, aiming to eliminate voltage control errors caused by system losses through capacitor power compensation. This enables zero steady-state error control of the bus voltage and increases the control accuracy of the system.

Thus, the control block diagram of the voltage outer loop based on direct power calculation proposed in this paper is illustrated in Fig. 6. The instantaneous values of the $\alpha$-$\beta$ axis components of the machine back-EMF, $e_\alpha$ and $e_\beta$, are indirectly obtained using Eqs. (4) and (5) based on the electrical angular velocity $\omega_e$, electrical angle $\theta_e$, and permanent magnet flux linkage $\psi_f$.

### 3.3. Comparison of Proposed and Conventional

The power inner loop of the system can be approximated as a first-order inertial element, with $T_p$ representing the time constant of this element. Figs. 7 and 8 show the control block diagrams of the bus voltage outer loop for the conventional PI control method and proposed control method, respectively. On one hand, according to Eq. (11):

$$P_1 = U_{dc} i_L + \frac{1}{2} C \frac{dU_{dc}^2}{dt} = \frac{U_{dc}^2}{R} + \frac{1}{2} C \frac{dU_{dc}^2}{dt} \tag{16}$$

From Eq. (16), it can be seen that the output power of the generator has a nonlinear relationship with the bus voltage, but a linear relationship with the square of the bus voltage. When conventional PI control method is used for bus voltage outer loop, the bus voltage itself is adopted as the control variable, without considering the nonlinear relationship between the generator output power and bus voltage. Consequently, the power control performance is poor. In contrast, the proposed method takes into account the linear relationship between generator output power and the square of the bus voltage. Based on practical physical significance, the feedback value of the capacitor energy storage is selected as the control variable for the outer loop, enabling linear control of the power inner loop. This approach is conducive to achieving high-performance control of the bus voltage.

On the other hand, conventional voltage outer loop control relies solely on voltage PI control. Due to the lag inherent in PI

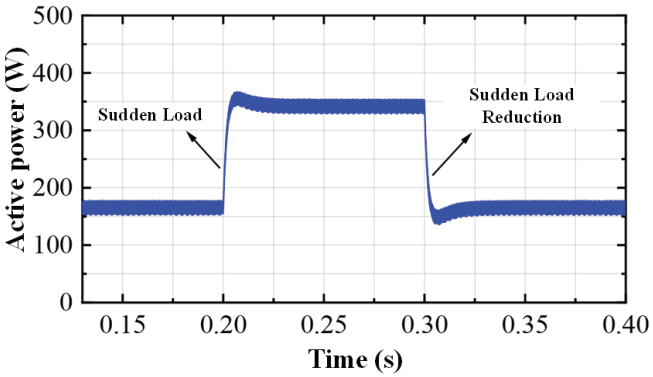


**FIGURE 9**. Dynamic simulation waveforms of system output active power under load variation using the conventional method.

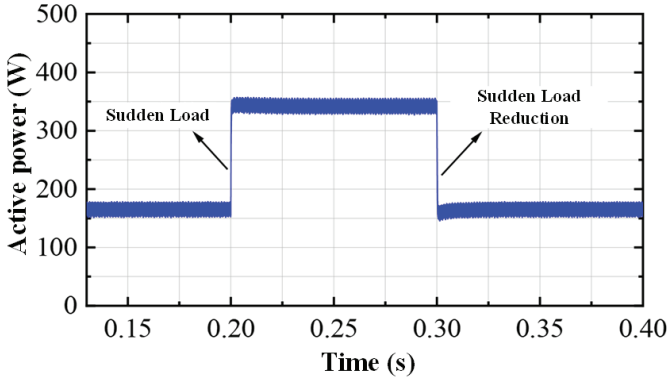


**FIGURE 10**. Dynamic simulation waveforms of system output active power under load variation using the proposed method.

control, when a sudden change occurs in the DC-side load, the bus voltage exhibits large fluctuations and slow recovery, resulting in poor dynamic performance. However, the proposed method is based on capacitor energy storage PI control and incorporates a feedforward of the DC-side power using load current and bus voltage information. Combined with the output of the capacitor energy storage PI controller, it allows for rapid acquisition of the reference value for the inner loop active power. The proposed method accelerates the response speed of the bus voltage and effectively enhances the system's ability to withstand load disturbances.

## 4. SIMULATION AND EXPERIMENTAL VERIFICATION

To verify the correctness and feasibility of the proposed voltage regulation control method based on direct power calculation, this paper uses a DTP-PMSG as the controlled object. Simulation and experimental validation are carried out for both the proposed method and conventional method according to the control block diagram shown in Fig. 6.

### 4.1. Simulation Analysis

The relevant parameters for system simulation are listed in Table 1, with DC bus reference voltage set to 80 V. To compare the anti-disturbance capabilities of the conventional method and proposed method, the load is set as a step load, and its value changes abruptly at a certain moment. Accordingly, the simulation scenarios are configured as follows: after the system starts and reaches steady state, a load of 160 W is suddenly applied at 0.2 s and then suddenly removed at 0.3 s. Figs. 9 and 10 show dynamic simulation waveforms of the system's output active power under step load increase and decrease for the conventional method and proposed method, respectively. The conventional method introduced approximately 8% overshoot in the bus voltage, while the proposed method produced almost none. As a result, the proposed method offers faster response speed and superior dynamic performance compared to the conventional approach.

**TABLE 1**. DTP-PMSG system parameters.

| Parameters | Values |
|---|---|
| Number of motor phases | 6 |
| Number of motor poles | 5 |
| Stator resistance $R_s$ ($\Omega$) | 0.67 |
| $d$-axis inductance $L_d$ (mH) | 2.46 |
| $q$-axis inductance $L_q$ (mH) | 2.46 |
| Magnetic flux amplitude of permanent magnet $\psi_f$ (Wb) | 0.0885 |
| DC bus capacitor $C$ ($\mu$F) | 2200 |
| DC bus voltage reference $U_{dc}$ (V) | 80 |
| Motor speed $N$ (r/min) | 750 |

Figure 11 compares dynamic waveforms of the bus voltage under the two control methods, and Table 2 provides a simulation-based comparison of their dynamic performance. Voltage fluctuation is defined as the absolute value of the difference between the maximum or minimum bus voltage and the reference voltage after a sudden load change. Recovery time is defined as the shortest time required for the bus voltage to return within $\pm 0.05$ V of the reference voltage following a sudden load change. The overshoot or undershoot of the bus voltage during load changes is caused by a mismatch between the generator output power and load power at the moment of load variation. Therefore, improving the dynamic performance of the bus voltage requires accelerating the response speed of the generator's output power. The faster the dynamic response of the generator's output power is during load changes, the better the dynamic performance of the bus voltage is, and the smaller the adverse impact of sudden load disturbances is on the system. Since the proposed method achieves a faster active power response than the conventional method, the proposed method effectively enhances the dynamic performance of the bus voltage compared to the conventional control method. Based on the comparison in Table 2, the proposed method reduces the amplitude of bus voltage fluctuations by approximately 70% and shortens recovery time by about 40% relative to the conventional method, demonstrating superior bus voltage control performance.

Additionally, to investigate the variation trends of the fast adjustment component and the error compensation component of the active power reference in the proposed method during sudden load changes, the simulation scenario is kept consis-

**TABLE 2**. Comparison of dynamic performance of bus voltage between conventional method and the proposed method.

| Control methods | Add/Reduce load | Voltage fluctuation | Fluctuation percentage | Recovery time |
|---|---|---|---|---|
| Conventional method | Add load | 1.16 V | 1.45% | 32 ms |
| | Reduce load | 1.17 V | 1.46% | 33 ms |
| Proposed method | Add load | 0.28 V | 0.35% | 18 ms |
| | Reduce load | 0.30 V | 0.38% | 20 ms |

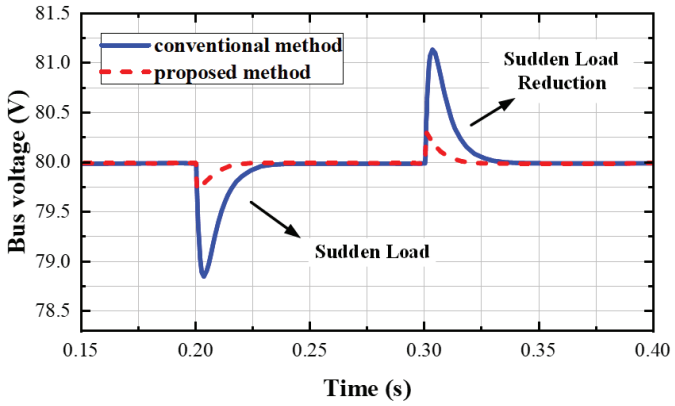


**FIGURE 11**. Comparison of dynamic bus voltage waveforms under load variation between the conventional and proposed methods.

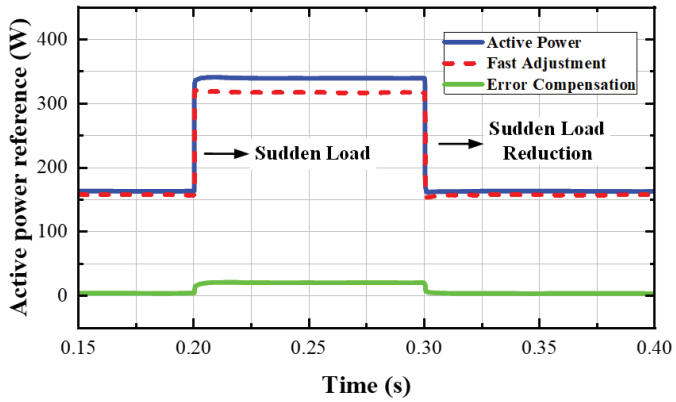


**FIGURE 12**. Variation trends of each active power reference component during load changes.

tent. Fig. 12 presents trends of the active power fast adjustment component and the error compensation component during the loading process. The active power reference consists of both the fast adjustment component and error compensation component, where the fast adjustment component dominates, and the error compensation component serves as an auxiliary adjustment. When a sudden load change occurs, the fast adjustment component is able to adjust quickly in response to the change in load state, exhibiting a rapid dynamic response. Meanwhile, the error compensation component increases or decreases according to the variation in system losses during the load change, which is consistent with theoretical analysis. The above simulation results indicate that, when sudden load changes are applied, the proposed fast voltage regulation strategy can improve the dynamic performance of the system bus voltage and effectively enhance the DC-side bus voltage disturbance rejection capability of the DTP-PMSG rectification system.

### 4.2. Test Verification

To further verify the correctness and feasibility of the proposed voltage regulation control method, a DTP-PMSG rectification system experimental platform was established in the laboratory, as shown in Fig. 13. To evaluate the anti-disturbance capability of the proposed method, a dynamic performance comparison with the conventional method is conducted by applying step changes to the load. The test conditions are set as follows. After system startup and reaching steady state, a load of 160 W is suddenly applied. Once the system stabilizes, the load is suddenly removed. The DC bus reference voltage is set to 80 V.

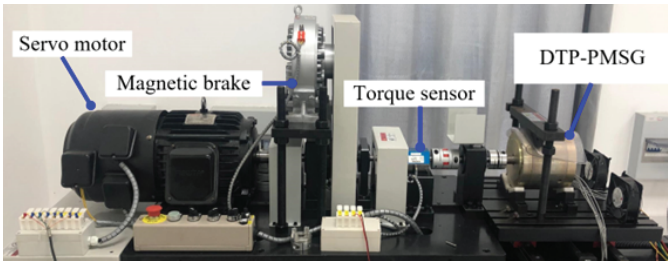


**FIGURE 13**. Experiment platform.

Figures 14 and 15 show the dynamic response waveforms for load addition and removal under the conventional method and proposed method, respectively. From top to bottom, the waveforms represent generator active power, reactive power, and bus voltage.

Table 3 provides a comparison of the dynamic performance between the two control methods. The definition of voltage fluctuation is the same as in the simulation, while recovery time is defined as the shortest time for the bus voltage to return within $\pm 0.4$ V of the reference voltage after a sudden load change.

In terms of bus voltage control, the proposed method enables the bus voltage to respond more rapidly to load disturbances than the conventional method. Both the amplitude of voltage fluctuation and recovery time are considerably reduced after a load change, demonstrating the superior dynamic performance of the proposed method. The proposed method reduces the amplitude of bus voltage fluctuation by approximately 50% and shortens recovery time by about 55% compared to the conventional method. Fig. 16 shows the variation of each com-

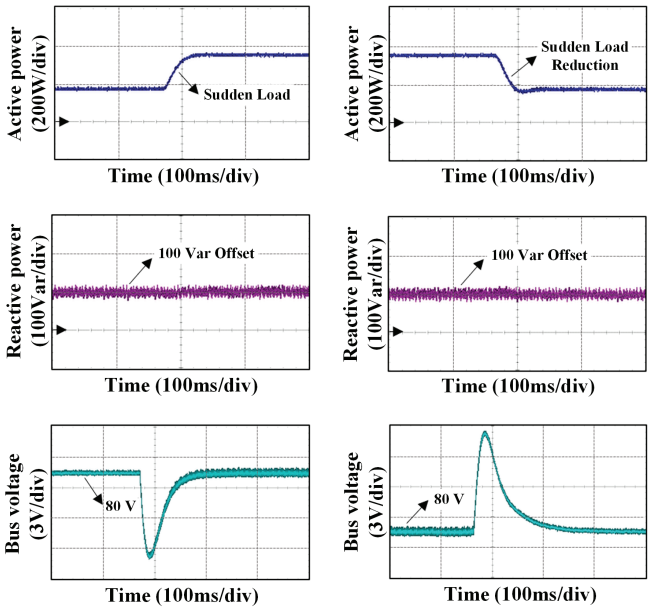


**FIGURE 14**. Experimental waveforms of load variation using the conventional control method.

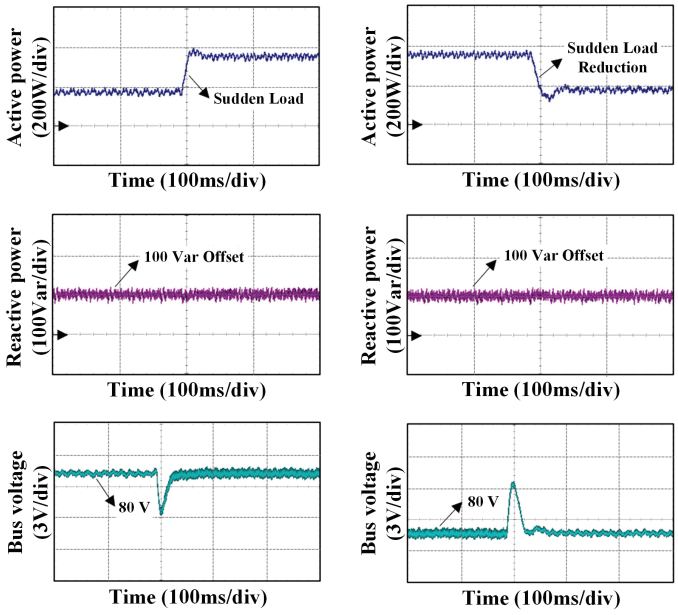


**FIGURE 15**. Experimental waveforms of load variation using the proposed control method.

**TABLE 3**. Comparison of system dynamic performance tests under two control methods.

| Control methods | Add/Reduce load | Voltage fluctuation | Fluctuation percentage | Recovery time |
|---|---|---|---|---|
| Conventional method | Add load | 8.4 V | 10.5% | 108 ms |
| | Reduce load | 10.3 V | 12.9% | 160 ms |
| Proposed method | Add load | 4.4 V | 5.5% | 50 ms |
| | Reduce load | 5.1 V | 6.4% | 72 ms |

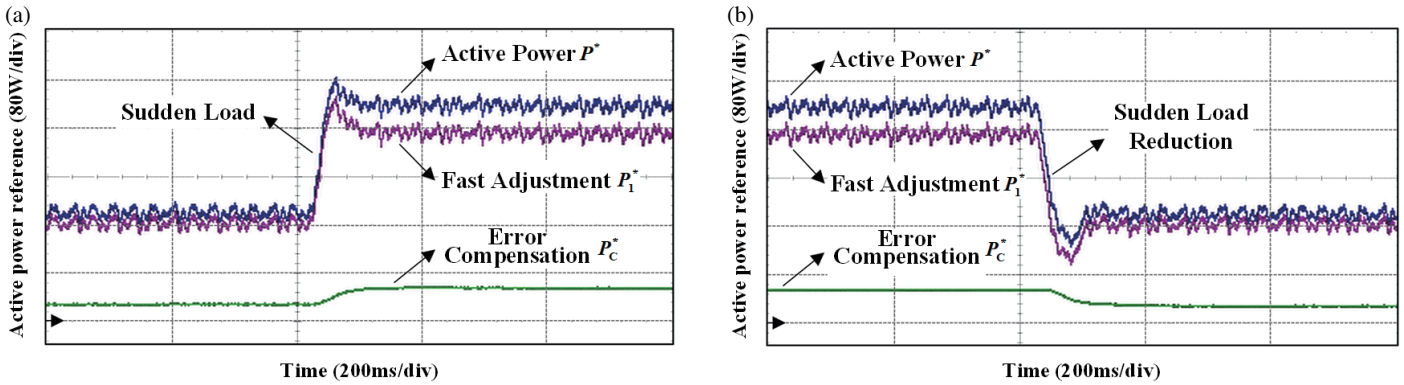


**FIGURE 16**. Schematic diagram of the variation of each component of the active power reference during load variation with the proposed method. (a) Sudden load. (b) Sudden load reduction.

ponent of the inner loop active power reference under sudden load changes. The active power reference $P^*$ consists of the fast adjustment component $P_1^*$ and error compensation component $P_C^*$. Under light load conditions, system loss is small, with $P_C^*$ around 30 W and $P_1^*$ about 160 W, making the fast adjustment component dominant. When a load is suddenly added, system loss increases, raising $P_C^*$ to 54 W, while $P_1^*$ quickly increases to 304 W in response to the sudden load, allowing the generator's output active power to rise rapidly and thus avoiding significant voltage drop. Conversely, when a load is suddenly removed, system loss decreases, lowering $P_C^*$ to 30 W, while $P_1^*$ quickly decreases to 160 W, enabling the generator's output active power to fall rapidly and preventing significant voltage overshoot.

To further validate the conclusions regarding parameter $T_C$, Fig. 17 presents the bus voltage response under different val-

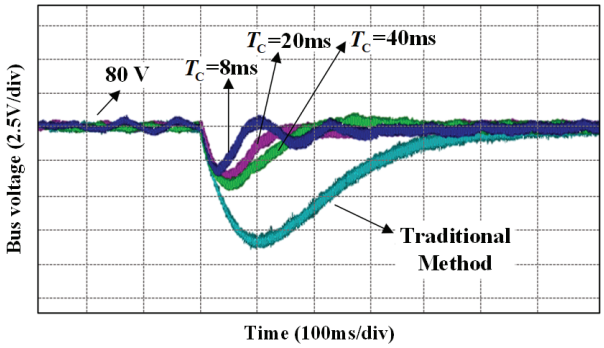


**FIGURE 17**. Experimental waveforms of sudden load application under different $T_C$ conditions.

ues of $T_C$ for a given operating condition during load addition. The proposed method consistently outperforms the conventional method in terms of bus voltage dynamic performance under step load changes. When the value of $T_C$ in the proposed method decreases, both the amplitude of bus voltage fluctuation and the recovery time are reduced, and the dynamic response speed increases. However, if $T_C$ is set too small, voltage oscillations may occur, reducing the relative stability of the system, which is consistent with the previous theoretical analysis. Considering both the dynamic response speed of the bus voltage and system stability, and based on the experimental conditions in this study, the optimal value for $T_C$ is determined to be 30 ms. The above dynamic experimental results indicate that the proposed fast voltage regulation control strategy based on direct power calculation can significantly improve the dynamic response of the voltage outer loop, suppress bus voltage fluctuations caused by sudden load changes, and enhance the DC-side bus voltage disturbance rejection capability of the DTP-PMSG system.

## 5. CONCLUSION

This paper proposes a fast voltage regulation control method for DTP-PMSG based on direct power calculation. On one hand, the voltage outer loop utilizes the generator power balance equation to directly compute the output of the voltage outer loop, thereby improving the dynamic response speed of the voltage regulation system and enabling adaptation to sudden load changes. On the other hand, capacitor power compensation is employed to eliminate control errors caused by system losses. The following conclusions are drawn from both software simulations and experimental results:

(1) In this study, the reference value for the power inner loop is directly obtained through the use of direct power calculation in the system's outer loop, which effectively enhances the dynamic performance of the bus voltage outer loop. Simultaneously, capacitor power compensation is adopted to achieve zero steady-state error control of the bus voltage, thereby improving the control accuracy of the system.

(2) Compared with the conventional PI control method for the voltage outer loop, the proposed method reduces the amplitude of bus voltage fluctuations by approximately 50% and shortens the voltage recovery time by about 55% when the system experiences sudden load increases or decreases. Thus, the proposed method contributes to improved dynamic performance of the bus voltage and enhances the system's ability to withstand load disturbances.

## ACKNOWLEDGEMENT

This work was supported in part by the Key Research and Development of Zhenjiang under Grant GY2023011, and in part by the China Post-doctoral Project under Grant 2022M721376.

## REFERENCES

[1] Ye, C., D. Yu, K. Liu, Y. Dai, C. Deng, J. Yang, and J. Zhang, "Research of a stator PM excitation solid rotor machine for flywheel energy storage system," *IEEE Transactions on Industrial Electronics*, Vol. 69, No. 12, 12 140–12 151, Dec. 2022.

[2] Sun, M., Y. Xu, and W. Zhang, "Multiphysics analysis of flywheel energy storage system based on cup winding permanent magnet synchronous machine," *IEEE Transactions on Energy Conversion*, Vol. 38, No. 4, 2684–2694, Dec. 2023.

[3] Yang, J., P. Liu, C. Ye, L. Wang, X. Zhang, and S. Huang, "Multidisciplinary design of high-speed solid rotor homopolar inductor machine for flywheel energy storage system," *IEEE Transactions on Transportation Electrification*, Vol. 7, No. 2, 485–496, Jun. 2021.

[4] Jiang, X., L. Zhang, F. Li, and S. Zhang, "Hybrid method for electromagnetic vibration calculation of flatted single-layer interior permanent magnet synchronous machines for flywheel application," *Progress In Electromagnetics Research C*, Vol. 150, 97–104, 2024.

[5] Gao, M., Z. Yu, W. Jiao, W. Hu, H. Geng, Y. Liu, S. Liu, and Y. Liu, "Study on electromagnetic performance of permanent magnet rotor and dual stator starter generator for electric vehicle range extender," *Progress In Electromagnetics Research B*, Vol. 106, 39–55, 2024.

[6] Zhang, W., A. Li, and J. Wang, "Design and evaluation of 5-DOF magnetic bearing system for saucer-shaped flywheel battery," *Progress In Electromagnetics Research C*, Vol. 143, 45–56, 2024.

[7] Xiang, Q., Z. Peng, and Y. Ou, "Study on electromagnetic vibration performance of hybrid excitation double stator BSRM for flywheel battery under eccentricity," *Progress In Electromagnetics Research C*, Vol. 126, 1–11, 2022.

[8] Zhang, Y., P. Yang, K. Cao, Y. Gao, G. Tang, and Q. Chen, "Improved model predictive torque control strategy incorporating decoupled sliding mode disturbance observer for PMSM," *Progress In Electromagnetics Research C*, Vol. 153, 105–117, 2025.

[9] Luo, W. and Z. Cheng, "Finite-control-set model predictive current closed-loop control based on prediction error compensation for PMSM," *Progress In Electromagnetics Research C*, Vol. 141, 163–173, 2024.

[10] Hoggui, A., A. Benachour, M. C. Madaoui, and M. O. Mahmoudi, "Comparative analysis of direct torque control with space vector modulation (DTC-SVM) and finite control set-model predictive control (FCS-MPC) of five-phase induction motors," *Progress In Electromagnetics Research B*, Vol. 108, 89–104, 2024.

[11] Zhang, Y., Y. Gao, K. Cao, P. Yang, G. Tang, and B. Luo, "Quasi-Z-source composite voltage vectors model predictive control with a novel sliding mode reaching law for PMSM,"

*Progress In Electromagnetics Research B*, Vol. 112, 75–87, 2025.

[12] Chen, Y., J. Yang, X. Zhang, L. Yan, and Y. Jia, "DC-Bus voltage control for FESSs with capacitor energy regulation and tracking differentiator," *IEEE Transactions on Transportation Electrification*, Vol. 11, No. 3, 8077–8090, Jun. 2025.

[13] Haque, M. M., M. S. Ali, P. Wolfs, and F. Blaabjerg, "A UPFC for voltage regulation in LV distribution feeders with a DC-link ripple voltage suppression technique," *IEEE Transactions on Industry Applications*, Vol. 56, No. 6, 6857–6870, Nov.–Dec. 2020.

[14] Yan, S., Y. Yang, S. Y. Hui, and F. Blaabjerg, "A review on direct power control of pulsewidth modulation converters," *IEEE Transactions on Power Electronics*, Vol. 36, No. 10, 11 984–12 007, Oct. 2021.

[15] Degioanni, F., I. G. Zurbriggen, and M. Ordonez, "Enhanced DC-link voltage dynamics for grid-connected converters," *IEEE Transactions on Industrial Electronics*, Vol. 69, No. 11, 10 787–10 796, Nov. 2022.

[16] Xiao, Q., X. Chen, Z. Cheng, Z. Tang, and Z. Yu, "A wide adaptation variable step-size adaline neural network parameter identification ipmsm model predictive control strategy," *Progress In Electromagnetics Research C*, Vol. 142, 85–94, 2024.

[17] Gui, Y., M. Li, J. Lu, S. Golestan, J. M. Guerrero, and J. C. Vasquez, "A voltage modulated DPC approach for three-phase PWM rectifier," *IEEE Transactions on Industrial Electronics*, Vol. 65, No. 10, 7612–7619, Oct. 2018.

[18] Gui, Y., F. Blaabjerg, X. Wang, J. D. Bendtsen, D. Yang, and J. Stoustrup, "Improved DC-link voltage regulation strategy for grid-connected converters," *IEEE Transactions on Industrial Electronics*, Vol. 68, No. 6, 4977–4987, Jun. 2021.

[19] Shen, X., C. Wu, Z. Liu, Y. Wang, J. I. Leon, J. Liu, and L. G. Franquelo, "Adaptive-gain second-order sliding-mode control of NPC converters via super-twisting technique," *IEEE Transactions on Power Electronics*, Vol. 38, No. 12, 15 406–15 418, Dec. 2023.

[20] Ran, H., W. Wei, and Y. Gao, "Design of permanent magnet synchronous wind power control system," *Progress In Electromagnetics Research C*, Vol. 139, 11–21, 2024.

[21] Fu, C., C. Zhang, G. Zhang, C. Zhang, and Q. Su, "Finite-time command filtered control of three-phase AC/DC converter under unbalanced grid conditions," *IEEE Transactions on Industrial Electronics*, Vol. 70, No. 7, 6876–6886, Jul. 2023.

[22] Shen, X., J. Liu, H. Lin, Y. Yin, A. M. Alcaide, and J. I. Leon, "Cascade control of grid-connected NPC converters via sliding mode technique," *IEEE Transactions on Energy Conversion*, Vol. 38, No. 3, 1491–1500, Sep. 2023.

[23] Jorge, S. G., J. A. Solsona, C. A. Busada, G. Tapia-Otaegui, A. S. Burguete, and M. I. M. Aguirre, "Nonlinear controller allowing the use of a small-size DC-link capacitor in grid-feeding converters," *IEEE Transactions on Industrial Electronics*, Vol. 71, No. 3, 2157–2166, Mar. 2024.

[24] Wai, R.-J. and Y. Yang, "Design of backstepping direct power control for three-phase PWM rectifier," *IEEE Transactions on Industry Applications*, Vol. 55, No. 3, 3160–3173, May-Jun. 2019.

[25] Liu, X., L. Qiu, J. Rodríguez, W. Wu, J. Ma, Z. Peng, D. Wang, and Y. Fang, "Neural predictor-based dynamic surface predictive control for power converters," *IEEE Transactions on Industrial Electronics*, Vol. 70, No. 1, 1057–1065, Jan. 2023.

[26] Ji, J., S. Jin, W. Zhao, D. Xu, L. Huang, and X. Qiu, "Simplified three-vector-based model predictive direct power control for dual three-phase PMSG," *IEEE Transactions on Energy Conversion*, Vol. 37, No. 2, 1145–1155, Jun. 2022.

[27] Zhang, Y., P. Yang, C. Liu, S. Li, K. Cao, Z. Liu, and Z. Cheng, "Improved model predictive torque control for PMSM based on anti-stagnation particle swarm online parameter identification," *Progress In Electromagnetics Research B*, Vol. 114, 51–66, 2025.